cell activation route or phenotype; instead it controls how rapidly and simultaneously cells initiate activation, allowing limited machinery to elicit wide-ranging responses.

Cytotoxic T lymphocytes (CTLs) are critical for immune defense against tumors and viral

state using the same transcriptional pathway. Thus, we show that stimulation strength dictates how rapidly and uniformly cells respond.

Results

Distinct transcriptional phases of early T cell activation

We first sought to characterize transcriptomic changes during the initial six hours of naive $CD8^+$ T cell activation by single-cell RNA-sequencing (scRNA-seq). We used the OT-I transgenic TCR model to facilitate strict control over the timing of antigen encounter and the strength of the activating stimulus. Cells were isolated from OT-I TCR transgenic Rag1-deficient mice, in which all peripheral $CD8^+$ T cells recognize the ovalbumin peptide SIINFEKL presented by the MHC class I molecule $H\text{-}2K^b$. Ex vivo $CD8^+$ OT-I T cells were stimulated with pure peptide for self-presentation to avoid contamination by antigen-presenting-cell RNA. By staining cells for surface protein expression before sorting into lysis buffer for scRNA-seq, we simultaneously measured expression of four surface proteins and quantified genome-wide mRNA in the same cells. We assayed one protein that is downregulated with activation, CD62L (L-selectin, encoded by *Sell*), and three proteins upregulated with activation, CD69, CD25 (encoded by *Il2ra*) and CD44.

We first profiled a time course of strong stimulation by sequencing the transcriptomes of individual OT-I $CD8^+$ T cells after 0, 1, 3 and 6 hours of activation with 1 •M of the high potency OT-I TCR cognate peptide SIINFEKL (N4) in the presence of IL-2 (Supplementary Fig. 1a and Methods). 87% of cells passed quality control filtering, resulting in 44-64 cells per condition. Protein profiles revealed a rapid drop in CD62L expression, followed by sequential increases in CD69, CD25 and CD44 expression (Fig. 1a). Surface protein measurements and principal components analysis applied to the mRNA data confirmed that, despite a uniform activation stimulus, these cells were heterogeneous during the first 6 hours of activation (Fig. 1a,b). Because of this diversity, simply grouping the cells by sampling time cannot achieve the fine resolution required to understand coordination of gene expression. Instead, we took advantage of the heterogeneity within each stimulation condition to order all cells by their progressively changing transcriptional profiles, referring to the progress in ‚pseudotime' instead of real time. We used a diffusion pseudotime method[31], a computational approach which finds the most direct path through the observed cell states based upon each cell's gene expression profile. Fitting a diffusion pseudotime trajectory to the single-cell transcriptomic data, we created a fine-grained map of activation (Fig. 1c, Supplementary Fig. 1b).

The distribution along pseudotime of all cells from the various time points revealed three clusters of resting, early activated and late activated cells (Fig. 1d, Supplementary Fig. 1c,d). We performed a differential expression analysis to compare each activated cluster to the resting cells. Cells in the early stages of activation primarily increased expression of genes involved in immune and regulatory processes, whereas cells in the later stages of activation showed strong upregulation of genes involved in metabolic and biosynthetic functions (Supplementary Table 1), which are critical for T cell effector differentiation[32,33]. We then examined genes differentially expressed in the early activation cluster compared to both the resting and late activation clusters to identify transient early expression changes. Filtering

for differentially expressed genes uniquely upregulated in early activation revealed an enrichment for genes that encode transcriptional regulators (enrichment value p value 1.8 x 10^{-9}, Fig. 1e, Supplementary Fig. 1e). In particular, the early response NR4A family orphan nuclear receptors, including *Nr4a1* (Nur77) whose expression has been found to reflect TCR signaling activity[27,34–36], were most highly expressed 1 hour after activation (Fig. 1f). Additionally, early growth response factors (*Egr1* and *Egr2*) and the AP-1 transcription factor subunit *Fosb* followed similar expression patterns. Thus, we identified two distinct phases of the activation response.

Ligand potency controls response rate of CD8^{+} T cells

To determine how TCR stimulation strength might affect this early response, we selected two transcription factors characteristic of the early activation profile, *Nr4a1* and *Fosb*, and examined their expression by RNA flow cytometry while modulating TCR signaling strength. We stimulated cells with each of four peptides with previously characterized potency for stimulating the OT-I TCR[37]: the cognate SIINFEKL peptide (N4); 2 variants

3a). To determine whether ligand potency controls transcriptional activation pathways, we combined data from cells stimulated for 6 hours with all ligands and the most potent ligand (N4) stimulation time course. 93% of cells in this combined data set passed quality control

stimulated with the medium potency (T4) ligand (Fig. 4b,c, Supplementary Fig. 3c,d). Although many genes, including *Ccl3* and *Ccl4* chemokines, have been previously observed to exhibit altered expression with weak ligand stimulation[15,28], here we demonstrate that this occurs for only a small subset of genes when we account for the activation status of the cells. Of particular importance, genes directing the metabolic and biosynthetic programs of T cell activation were not enriched in our differentially expressed gene lists, suggesting that all activated cells, regardless of ligand potency, can mount these energetic effector differentiation processes. Likewise, early transcription of *Gzmb*, encoding the important cytolytic effector molecule Granzyme B, did not significantly differ between stimulation conditions when accounting for cellular activation status (Supplementary Fig. 3e). Our results indicate that while there are specific genes involved in leukocyte recruitment and endogenous peptide presentation whose expression depends on ligand strength, the overwhelming majority of genes expressed in early activation depend on activation status and not the potency of the stimulus.

Activated T cells achieve the same spectrum of effector phenotypes regardless of stimulation potency

Having observed that, regardless of the primary stimulus, activated T cells progress along the same transcriptomic activation trajectory, we next examined whether cells exhibited phenotypic differences associated with stimulation strength during the first two days of effector T cell differentiation. Because OTI T cells can undergo extensive death when activated with soluble peptide for multiple days, we instead used peptide-pulsed APCs to activate naive T cells for two days (Supplementary Fig. 4a). In this system, we observed negligible activation after two days by the low potency (G4) peptide (Fig. 5a). This is in contrast to pure peptide stimulation with low potency ligand, which, consistent with our observations of transcriptional activity at 6 hours, drove full activation at two days (Supplementary Fig. 4b). Ex vivo $CD8^+$ OT-I T cells were stimulated in IL-2-supplemented media with autologous T-depleted splenocytes (cells remaining after $CD8^+$ T cell isolation) pulsed with one of the 4 peptides used in our transcriptomic studies or Q4H7 peptide, whose potency for stimulating OT-I T cells lies between that of T4 and G4 peptides (medium-low potency). After 2 days of activation, the majority of T cells stimulated with the three strongest ligands (N4, T4, Q4H7) were proliferating (Fig. 5a). The proportion of cells in later division cycles and the total number of T cells were associated with stimulation strength (Fig. 5b,c), in agreement with previous observations suggesting an increased percentage of proliferating cells, shorter time to first division, or greater proliferation with stronger TCR-pMHC interactions[11,12,14,16,19,21,27]. However, we noted that the most proliferative cells in each condition that stimulated proliferation had all undergone 4 divisions, indicating that the few cells that began proliferating immediately after stimulation with weaker ligands were not slower to divide. Although it has been previously reported that stimulation strength affects the proportion of proliferating cells and the time to first division[22], our results now show that weaker ligands do not cause a universal delay in proliferation, but rather reduce the number of cells that activate immediately. Together with our results from early activation transcriptomic analysis, we conclude that ligand potency determines the rate with which an individual cell initiates activation and thus the heterogeneity of activation across the population.

Proliferation represents only one component of effector differentiation, and expression of cytokines, cytotoxic mediators, and costimulatory or co-inhibitory receptors can control the phenotype of differentiated CTLs. In order to examine effector phenotypes without making prior assumptions about which proteins would be co-expressed, we used mass cytometry to simultaneously measure 19 surface and intracellular proteins related to T cell differentiation and effector function. After two days of stimulation with peptide-pulsed autologous T-depleted splenocytes, we tested for subpopulations of cells that changed in abundance[39] under stimulation with any ovalbumin peptide variant compared to the null peptide NP68. The high-dimensional space defined by the 19 measured proteins was divided into phenotypic hyperspheres and the abundance of cells from each condition was quantified within each hypersphere (Fig. 6a). We identified phenotypic hyperspheres that differed significantly in abundance in any peptide stimulation condition (Fig. 6b). Examination of protein expression profiles that defined each phenotype revealed that, similar to its proliferation profile, the least potent ligand (G4) stimulated only a very small proportion of cells to transition from a $CD44^{lo}CD62L^{hi}$ naive phenotype to a $CD44^{hi}CD62L^{lo}$ effector phenotype (Fig. 6c, Supplementary Fig. 5). In contrast, stronger ligands (N4, T4, and Q4H7) drove increased abundance of effector populations co-expressing many effector-associated proteins including the high affinity IL-2 receptor subunit CD25, the cytotoxic mediator Granzyme B, the coinhibitory receptor CTLA-4, and the transcription factor T-bet that promotes effector $CD8^{+}$ T cell differentiation. This effector phenotype was present in all activated populations, regardless of the potency of the primary stimulus, and was validated for a subset of proteins by flow cytometry (Supplementary Fig. 6a,b). Granzyme B expression levels in Granzyme B^{+} cells were marginally reduced with the highest potency stimulus (N4) (Supplementary Fig. 6c,d), as observed previously in vivo[8], but in contrast to that previous study, we did not observe a decrease in the percentage of Granzyme B^{+} cells with strong stimulation (Supplementary Fig. 6b). Of note, IFN-γ was not expressed in all effector T cells after two days of stimulation, instead emerging in a small subset of cells (up to 20%) primarily under stimulation with ligands of medium/medium-low potency (T4 or Q4H7) (Supplementary Fig. 6e-g). Divergence of IFN-γ expression from other effector phenotypes was noted in an earlier study[14], however, its infrequent expression in effector cells and disconnect from other effector protein phenotypes suggests that IFN-γ is not representative of cytolytic effector cell differentiation in this system.

We verified effector protein expression phenotypes using wild-type splenocytes as APCs (Supplementary Fig. 4c,d). Under wild-type APC activation, G4 stimulation activated a small population of cells. These activated cells behaved similarly to those activated by other primary stimuli. Together, our phenotypic profiling supports a model in which ligand potency determines the rate with which cells embark on effector differentiation but not the spectrum of effector phenotypes they can achieve.

All differentiated effector cells are cytolytic

The main effector function of CTLs is the targeted release of cytolytic granules upon encountering an antigen-presenting target cell. Cytolytic granules carry the lysosome-associated transmembrane protein LAMP1, which enables measurement of degranulation in individual cells via the quantity of LAMP1 transiently trafficked to the cell surface during

antigen challenge. To test how the TCR-pMHC affinity of a cell*ƒ*s primary stimulus might

autocrine and paracrine availability of the cytokine IL-2 modulates T cell activation and proliferation[11,14,16,24,27,28,44] through PI3K and Myc activity[18,26,33,45], and weak stimulation can result in insufficient IL-2 to support a proliferative response[11,16,27,33,46]. However, IL-2 secreted by activated $CD4^+$ and $CD8^+$ T cells would likely be expressed in the lymphoid tissue microenvironment in a physiological, polyclonal response, and cells stimulated by weak ligands can co-opt IL-2 from co-cultured cells stimulated by strong ligands[26]. Variations between experimental protocols pertaining to these factors have left the field unclear as to whether cell-intrinsic ligand strength-dependent T cell phenotypes exist. We demonstrate that in a controlled cellular environment, all activated cells can achieve an effector phenotype via shared transcriptional machinery.

Previous in vivo cytotoxicity studies have demonstrated reduced total killing by CTLs induced by low potency ligands[8,9,12]. However, two reports noted that, early after activation, low potency stimulation resulted in greater cytolytic capacity per cell compared to high potency stimulation[8,9]. Strongly stimulated T cells were instead retained in the periarteriolar lymphoid sheaths of the spleen[9] or in the interfollicular regions of the lymph node in a CXCR3-dependent manner[8], reducing their availability for killing. In our data, RNA expression of *Cxcr3* exhibited a non-significant trend toward downregulation in G4-stimulated cells after accounting for activation status at 6 hours (Supplementary Table 2), and genes encoding other chemokines and receptors were upregulated with high potency stimulation, suggesting additional potential mechanisms. In contrast, in an ex vivo killing assay, CTLs generated in vivo with high or low potency ligands in the presence of exogenous IL2 exhibited comparable cytotoxicity[28]. In our controlled in vitro system, we find that all T cells that achieve an effector phenotype are cytolytically competent, suggesting that large divergences observed in vivo are not intrinsic to the T cell response to TCR stimulation.

Ligand potency can affect TCR-induced signaling events upstream of transcription including calcium fluxes[47,48], TCR-coreceptor interaction[42], post-translational modifications of signaling cascade components[5,13,17,19,29,42], and transcription factor nuclear translocation[13]. Such signaling mechanisms may drive the altered rate of transcription initiation that we have identified[49]. It is interesting to consider what might cause specific cells to be the first to respond, particularly to low potency stimulation. CD8 and SHP-1 (encoded by *Ptpn6*) protein expression levels and markers of metabolic activity are associated with response propensity in mature OT-I[50] and naive T cells[21], respectively. Unfortunately, due to the destructive nature of the single-cell sequencing technologies, cells cannot be comprehensively profiled both before and after activation. Hypothesis-driven sorting experiments may be fruitful in identifying additional markers of poised cells, but ideally a genome-wide screening experiment would be required to understand all contributing factors.

Our results emphasize the importance of using single-cell approaches to measure highly heterogeneous systems and identify rate-based responses[46]. These methods have allowed us to examine the coordination of mRNA and protein phenotypes in individual cells to answer a fundamental question in T cell biology: how does stimulation strength control the cell-intrinsic naive T cell response? We demonstrate that the primary effect of ligand affinity is to

control the rate with which naive T cells initiate activation, not to lower effector gene expression within activated cells or drive the use of alternative transcriptional pathways. Additional environmental cues dependent on the nature of the antigen and other responding immune cell populations can adjust the ultimate phenotype of each clonal T cell response, but none of these characteristics is intrinsically determined by TCR signal strength. Indeed, the fact that heterogeneous, low efficiency T cell activation responses can achieve full effector phenotype and function via induction of the same genes that mediate synchronous responses to high potency ligands would seem fundamental to maintaining flexibility and sensitivity in the immune system. Using response rate to modulate clonal population size according to ligand strength makes use of common transcriptional machinery while allowing high affinity clones to become the most prevalent and suppressing low affinity clones with a near-zero activation rate. This model provides a mechanism by which peripheral $CD8^+$ T cells can generate a full CTL response to a vast range of peptide antigens with a finite set of rearranged receptors and signaling components.

Methods

Mice

Mice were bred and housed in the University of Cambridge CBS facility. The genotype of OT-I Rag-deficient mice (OT-I $Rag1^{tm1Bal}$ on a C57BL/6 background) was confirmed prior to study. The wild-type C57BL/6N mouse line was obtained from the Wellcome Trust Sanger Institute Mouse Genetics Project (Sanger MGP).

Cell culture

The murine lymphoblast EL4 cell line, originally from the Sir William Dunn School of Pathology Cell Bank, Oxford, was maintained in DMEM (Gibco) supplemented with 10% fetal bovine serum (Biosera) and penicillin-streptomycin (Sigma) and tested negative for mycoplasma.

Dissected spleens from OT-I Rag1-deficient mice were homogenized through a 70 •m filter. $CD8^+$ T cells were isolated using the CD8a+ T Cell Isolation Kit, mouse (Miltenyi). T cells were stimulated either with addition of purified peptide or with pulsed APCs. T-depleted OT-I splenocytes (the positive fraction from CD8a+ T cell separation) were used as APCs. Results were confirmed using wild-type splenocytes treated with RBC lysis buffer (eBioscience) as APCs. APCs were irradiated with ~3000 rad and pulsed for 2 hours with peptide before washing and co-culture with isolated T cells. OT-I APCs were cultured at a 5:1 ratio and wild-type APCs at a 2.5:1 ratio with T cells. Where indicated, T cells were stained with proliferation dye eFluor450 (eBioscience) according to the manufacturer*f*s instructions before culture. Cells were cultured in media composed of complete RPMI 1640 medium (Gibco), 10% fetal bovine serum (Biosera), penicillin-streptomycin (Sigma), sodium pyruvate (Gibco), L-glutamine (Sigma), b-mercaptoethanol (Gibco), and, unless indicated otherwise, 20 ng/mL („ 100 U/mL) murine IL-2 (Peprotech). The following peptides were used for stimulation at 1 •M unless otherwise indicated: SIINFEKL (N4), SIITFEKL (T4), SIIQFEHL (Q4H7), SIIGFEKL (G4), and ASNENMDAM (NP68) (Cambridge Bioscience). Although 1 •M is a higher concentration than required for

maximal activation of OT-I cells with pure N4 peptide[11,17,33], we sought to keep this variable constant across all ligands including G4 for which 1 •M was required to maximize induction of CD69 expression[19]. We observed no inhibitory effect of excess N4 peptide on early activation protein phenotypes (Supplementary Fig. 1a).

The rate of activation in response to the lowest potency ligand G4 differed between pure peptide and peptide-pulsed APC antigen presentation systems. Under pure peptide stimulation, G4 peptide was capable of activating transcription in approximately half of cells after 6 hours and by two days had activated proliferation in the whole population (Fig. 2,3 and Supplementary Fig. 4b). In contrast, G4-pulsed APCs induced negligible proliferation at two days (Fig. 5 and Supplementary Fig. 4c). These differences may be due to concentration and chronicity of antigen presentation, such that changing the antigen presenting system shifts the rate with which each ligand activates T cells but does not affect the ordering of these rates or the observation that all stimulation conditions capable of driving T cell activation use similar machinery. Our model in which ligand potency intrinsically determines relative activation rate is consistent with all of these observations.

Sorting for single-cell RNA-seq

Isolated naive OT-I T cells were stained with proliferation dye eF450. 5×10^4 cells per well were stimulated with 1 •M peptide in 200 •L media in 96-well round-bottom plates. Cells were washed in PBS, blocked with FcR blocking antibody (clone 93, Biolegend) and stained with Zombie Aqua (Biolegend), anti-CD8a eVolve 655 (clone 53-6.7, eBioscience), anti-CD44 APC-eFluor780 or APC-FIRE750 (clone IM7, eBioscience or Biolegend, respectively), anti-CD62L PE (clone MEL-14, eBioscience), anti-CD25 Alexa Fluor 488 (clone PC61.5, eBioscience), and anti-CD69 APC (clone H1.2F3, eBioscience). Anti-CD154 PE-Cy7 (clone MR1, Biolegend) and anti-CD71 PerCP-Cy5.5 (clone R17217, Biolegend) were also included in one experiment, but expression levels were largely invariant and therefore not included in the analysis. Cells were sorted on a BD Influx (BD Biosciences), selecting live cells that expressed CD8 and that had not proliferated (Supplementary Fig. 8a). We did not see proliferation at the time points used for scRNA-seq. Expression of all surface proteins was recorded for each indexed cell. Two scRNA-seq experiments were performed: experiment 1 consisted of 2 96-well plates of cells stimulated with the various peptides for 6 hours; experiment 2 consisted of 4 96-well plates of cells stimulated with N4, T4, G4, or

well before reverse transcription with SuperScript II (Invitrogen). cDNA amplification was performed with 23 PCR cycles and the resulting PCR products purified with Ampure XP Beads (Agencourt) at a volume ratio of 0.7:1 beads:DNA. Libraries were prepared using the

situation in which a root cell was not automatically identified from this condition, pseudotime was fit to only the subset of cells from the most and least stimulated conditions to find a root cell, and this cell was subsequently used as root in the full analysis. Clustering along pseudotime was performed using the classInt package for 1-dimensional class interval selection using the …jenks† method. To identify the most biologically variable genes among unstimulated cells, we first used the trendVar function of the scran Bioconductor package to fit a parametric curve followed by loess smoothing (span = 0.95) to the variance versus the mean log-expression of the spike-in transcripts. Biological variances of endogenous genes were then obtained by decomposing the variance using the decomposeVar function.

Isolated naive OT-I T cells were stimulated with 1 •M peptide for 0-6 hours in complete media as in the scRNA-seq experiment. After stimulation, cells were immediately moved to ice before RNA flow cytometry was performed using the PrimeFlow system (Thermo Fisher Scientific). Cell surfaces were stained with Zombie Aqua Fixable Viability Kit (Biolegend) before fixation and permeabilization. Cells were stained with *Nr4a1*AF568, *Fosb*AF647, and *Rpl39*AF488. Data were acquired on a BD LSRFortessa and analyzed in FlowJo (Supplementary Fig. 8b).

0.5, and differential abundance was analyzed using the edgeR Bioconductor package with a quasi-likelihood GLM fit[62] including the mouse of origin as a blocking factor for each sample. Significant hyperspheres were identified by analysis of deviance to detect those with differential abundance in any condition, controlling the spatial FDR at 5%. A t-SNE plot was generated using the Rtsne package[63] with a perplexity value of 50.

Flow cytometry

FC receptors were blocked with anti-mouse CD16/32 (clone 93, Biolegend) before staining. Dead cells were identified using the Zombie Aqua Fixable Viability Kit (Biolegend). Cells were stained with the following antibody clones: anti-mouse CD8a (clone 53-6.7, Biolegend), anti-mouse/human CD44 (clone IM7, Biolegend), anti-mouse CD62L (clone MEL-14, eBioscience), anti-mouse/human Granzyme B (clone GB11, Biolegend), anti-mouse CTLA4 (clone UC1-4B9, Biolegend), anti-mouse CD25 (clone PC61.5, eBioscience), and anti-mouse IFN-γ (clone XMG1.2, Biolegend). Intracellular staining of Granzyme B, CTLA-4, and IFN-γ was performed using the Foxp3/Transcription Factor Staining Buffer Set (eBioscience). To count cells, 123count eBeads (eBioscience) were added to flow cytometry tubes immediately before flow cytometer acquisition. Data was acquired on a BD LSRFortessa and analyzed in FlowJo. Cells were gated for size, single cells, living cells, and $CD8^+$ cells before examination of proliferation curves (Supplementary Fig. 8c). Cells were further gated on proliferation dye^+ cells to exclude any $CD8^-$ T cells in the APC fraction before quantification of division numbers and examination of surface and intracellular proteins. Statistical analyses of results from separate mice were performed using GraphPad Prism software.

Degranulation assay

Activated T cells were assayed for degranulation upon challenge with ovalbumin (N4)-pulsed EL4 cells or antibody-based TCR stimulation. Cells were stained with proliferation dye eFluor 450 (eBioscience) before stimulation to measure this parameter in degranulating cells. For cellular challenge, EL4 cells were pulsed with 1 •M of the highest potency N4 peptide for 1 hour and washed. Un-pulsed EL4 cells were used as a control. T cell stimulation cultures were mixed 1:1 with EL4 cells in media supplemented with anti-mouse LAMP1 PE (clone eBio1D4B, eBioscience, 2 •g/mL). For antibody-based challenge, CTLs were cultured on plates coated with 1 •M anti-CD3 (clone 145-2C11, BD Biosciences) for 1 hour at 37 ‡C. After 3 hours, cells were stained on ice. FC receptors were blocked with anti-mouse CD16/32 (clone 93, Biolegend) and cells were stained with the Zombie Aqua Fixable Viability Kit (Biolegend) and antibodies to CD8a (53-6.7, Biolegend) and CD44 (IM7, Biolegend). Data were acquired immediately on a BD LSRFortessa and analyzed in FlowJo. Cells were gated for size, single cells, living cells, and $CD8^+$ cells before examination of LAMP1 surface trafficking (Supplementary Fig. 8d,e). For samples activated for 2 days before degranulation testing, cells were also gated on $proliferation\ dye^+$ cells to exclude any T cells in the residual irradiated APC population where necessary. Where possible, samples were run in duplicate and measurements averaged. Statistical analyses of results from separate mice were performed using GraphPad Prism software.

Killing assay

After 8 days of activation, activated T cells were assayed for their ability to kill ovalbumin (N4)-pulsed EL4 cells. Cells were plated at T:EL4 cell ratios ranging from 10:1 to 0.3125:1 in round-bottom 96-well plates in RPMI without phenol red (Gibco), supplemented with 2% fetal bovine serum. EL4 cells without ovalbumin pulse were used as a control. Maximum death was estimated by adding lysis buffer to the same number of EL4 cells. All conditions were performed in duplicate. Cells were co-cultured for 3 hours and EL4 cell death assessed by lactate dehydrogenase (LDH) release using the CytoTox 96 Non-Radioactive Cytotoxicity Assay (Promega). Absorbances at 490nm were read on a VersaMax microplate reader (Molecular Devices) using SoftmaxPro 5.4.1 software. Changes in absorbance between wells containing pulsed and un-pulsed EL4 wells were calculated and compared to maximum EL4 death. Statistical analyses of results from separate mice were performed using GraphPad Prism software.

Supplementary Material

Refer to Web version on PubMed Central for supplementary material.

Acknowledgements

This work was funded by an MRC Skills Development Fellowship to ACR (MR/P014178/1); the Wellcome Trust, grants [103930] and [100140] to GMG; Cancer Research UK, core funding to JCM [A17197]; EMBL, core funding to JCM; the University of Cambridge; and Hutchison Whampoa Limited. Single cell collection and analysis was supported through MRC Clinical Research Infrastructure funds for the Cambridge Single Cell Facility (MR/M008975/1). WWYL and BG were supported by Bloodwise (12029) and Cancer Research UK (C1163/A12765 and C1163/A21762). This research was supported by the CIMR Flow Cytometry Core Facility. In particular, we wish to thank R. Schulte and C. Cossetti for their advice and support in cell sorting. We would also like to thank the CRUK-CI Flow Cytometry core, particularly M. Strzelecki and R. Grenfell, and Genomics core for their resources and assistance. We thank the Wellcome Trust Sanger Institute Mouse Genetics Project (Sanger MGP) and its funders for providing the wild-type C57BL/6 mouse line; funding information may be found at www.sanger.ac.uk/mouseportal
We thank C. Gawden-Bone, J. Warland, A. Denton and G. Frazer for critical reading of the manuscript.

References

1. Brownlie RJ, Zamoyska R. T cell receptor signalling networks: branched, diversified and bounded. Nat Rev Immunol. 2013; 13:257€269. [PubMed: 23524462]
2. Cantrell D. Signaling in lymphocyte activation. Cold Spring Harb Perspect Biol. 2015; 7
3. Conley JM, Gallagher MP, Berg LJ. T Cells and Gene Regulation: The Switching On and Turning Up of Genes after T Cell Receptor Stimulation in CD8 T Cells. Front Immunol. 2016; 7:76. [PubMed: 26973653]
4. Zikherman J, Au-Yeung B. The role of T cell receptor signaling thresholds in guiding T cell fate decisions. Curr Opin Immunol. 2015; 33:43€48. [PubMed: 25660212]

9. Zehn D, Lee SY, Bevan MJ. Complete but curtailed T-cell response to very low-affinity antigen. Nature. 2009; 458:211€214. [PubMed: 19182777]
10. Skokos D, et al. Peptide-MHC potency governs dynamic interactions between T cells and dendritic cells in lymph nodes. Nat Immunol. 2007; 8:835€844. [PubMed: 17632517]
11. Denton AE, et al. Affinity thresholds for naive CD8+ CTL activation by peptides and engineered influenza A viruses. J Immunol. 2011; 187:5733€5744. [PubMed: 22039305]
12. King CG, et al. T cell affinity regulates asymmetric division, effector cell differentiation, and tissue pathology. Immunity. 2012; 37:709€720. [PubMed: 23084359]
13. Palmer E, Drobek A, Stepanek O. Opposing effects of actin signaling and LFA-1 on establishing the affinity threshold for inducing effector T-cell responses in mice. Eur J Immunol. 2016; 46:1887€1901. [PubMed: 27188212]
14. Auphan-Anezin N, Verdeil G, Schmitt-Verhulst AM. Distinct thresholds for CD8 T cell activation lead to functional heterogeneity: CD8 T cell priming can occur independently of cell division. J Immunol. 2003; 170:2442€2448. [PubMed: 12594268]
15. Man K, et al. The transcription factor IRF4 is essential for TCR affinity-mediated metabolic programming and clonal expansion of T cells. Nat Immunol. 2013; 14:1155€1165. [PubMed: 24056747]
16. Marchingo JM, et al. T cell signaling. Antigen affinity, costimulation, and cytokine inputs sum linearly to amplify T cell expansion. Science. 2014; 346:1123€1127. [PubMed: 25430770]
17. Navarro MN, Feijoo-Carnero C, Arandilla AG, Trost M, Cantrell D 42inputs sum

31. Haghverdi L, Buttner M, Wolf FA, Buettner F, Theis FJ. Diffusion pseudotime robustly reconstructs lineage branching. Nat Methods. 2016; 13:845€848. [PubMed: 27571553]
32. Pollizzi KN, Powell JD. Integrating canonical and metabolic signalling programmes in the regulation of T cell responses. Nat Rev Immunol. 2014; 14:435€446. [PubMed: 24962260]
33. Tan TCJ, et al. Suboptimal T-cell receptor signaling compromises protein translation, ribosome biogenesis, and proliferation of mouse CD8 T cells. Proc Natl Acad Sci U S A. 2017; 114:E6117€E6126. [PubMed: 28696283]
34. Moran AE, et al. T cell receptor signal strength in Treg and iNKT cell development demonstrated by a novel fluorescent reporter mouse. J Exp Med. 2011; 208:1279€1289. [PubMed: 21606508]
35. Ashouri JF, Weiss A. Endogenous Nur77 Is a Specific Indicator of Antigen Receptor Signaling in Human T and B Cells. J Immunol. 2017; 198:657€668. [PubMed: 27940659]
36. Au-Yeung BB, et al. A sharp T-cell antigen receptor signaling threshold for T-cell proliferation. Proc Natl Acad Sci U S A. 2014; 111:E3679€3688. [PubMed: 25136127]
37. Alam SM, et al. Qualitative and quantitative differences in T cell receptor binding of agonist and antagonist ligands. Immunity. 1999; 10:227€237. [PubMed: 10072075]
38. Moreau HD, et al. Dynamic in situ cytometry uncovers T cell receptor signaling during immunological synapses and kinapses in vivo. Immunity. 2012; 37:351€363. [PubMed: 22683126]
39. Lun ATL, Richard AC, Marioni JC. Testing for differential abundance in mass cytometry data. Nat Methods. 2017
40. Prlic M, Hernandez-Hoyos G, Bevan MJ. Duration of the initial TCR stimulus controls the magnitude but not functionality of the CD8+ T cell response. J Exp Med. 2006; 203:2135€2143. [PubMed: 16908626]
41. van Stipdonk MJ, et al. Dynamic programming of CD8+ T lymphocyte responses. Nat Immunol. 2003; 4:361€365. [PubMed: 12640451]
42. Yachi PP, Ampudia J, Zal T, Gascoigne NR. Altered peptide ligands induce delayed CD8-T cell receptor interaction--a role for CD8 in distinguishing antigen quality. Immunity. 2006; 25:203€211. [PubMed: 16872849]
43. Zahm CD, Colluru VT, McNeel DG. Vaccination with High-Affinity Epitopes Impairs Antitumor Efficacy by Increasing PD-1 Expression on CD8+ T Cells. Cancer Immunol Res. 2017; 5:630€641. [PubMed: 28634215]
44. Pipkin ME, et al. Interleukin-2 and inflammation induce distinct transcriptional programs that promote the differentiation of effector cytolytic T cells. Immunity. 2010; 32:79€90. [PubMed: 20096607]
45. Heinzel S, et al. A Myc-dependent division timer complements a cell-death timer to regulate T cell and B cell responses. Nat Immunol. 2017; 18:96€103. [PubMed: 27820810]
46. Tkach KE, et al. T cells translate individual, quantal activation into collective, analog cytokine responses via time-integrated feedbacks. Elife. 2014; 3:e01944. [PubMed: 24719192]
47. Chen JL, et al. Ca2+ release from the endoplasmic reticulum of NY-ESO-1-specific T cells is modulated by the affinity of TCR and by the use of the CD8 coreceptor. J Immunol. 2010; 184:1829€1839. [PubMed: 20053942]
48. Le Borgne M, et al. Real-Time Analysis of Calcium Signals during the Early Phase of T Cell Activation Using a Genetically Encoded Calcium Biosensor. J Immunol. 2016; 196:1471€1479. [PubMed: 26746192]
49. Mayya V, Dustin ML. What Scales the T Cell Response? Trends Immunol. 2016; 37:513€522. [PubMed: 27364960]
50. Feinerman O, Veiga J, Dorfman JR, Germain RN, Altan-Bonnet G. Variability and robustness in T cell activation from regulated heterogeneity in protein levels. Science. 2008; 321:1081€1084. [PubMed: 18719282]
51. Picelli S, et al. Full-length RNA-seq from single cells using Smart-seq2. Nat Protoc. 2014; 9:171€181. [PubMed: 24385147]
52. Liao Y, Smyth GK, Shi W. The Subread aligner: fast, accurate and scalable read mapping by seed-and-vote. Nucleic Acids Res. 2013; 41:e108. [PubMed: 23558742]

53. Liao Y, Smyth GK, Shi W. featureCounts: an efficient general purpose program for assigning sequence reads to genomic features. Bioinformatics. 2014; 30:923€930. [PubMed: 24227677]
54. Lun AT, McCarthy DJ, Marioni JC. A step-by-step workflow for low-level analysis of single-cell RNA-seq data with Bioconductor. F1000Res. 2016; 5:2122. [PubMed: 27909575]
55. McCarthy DJ, Campbell KR, Lun AT, Wills QF. Scater: pre-processing, quality control, normalization and visualization of single-cell RNA-seq data in R. Bioinformatics. 2017; 33:1179€1186. [PubMed: 28088763]
56. Lun ATL, Calero-Nieto FJ, Haim-Vilmovsky L, Gottgens B, Marioni JC. Assessing the reliability of spike-in normalization for analyses of single-cell RNA sequencing data. Genome Res. 2017; 27:1795€1806. [PubMed: 29030468]
57. Johnson WE, Li C, Rabinovic A. Adjusting batch effects in microarray expression data using empirical Bayes methods. Biostatistics. 2007; 8:118€127. [PubMed: 16632515]
58. McCarthy DJ, Chen Y, Smyth GK. Differential expression analysis of multifactor RNA-Seq experiments with respect to biological variation. Nucleic Acids Res. 2012; 40:4288€4297. [PubMed: 22287627]
59. Robinson MD, McCarthy DJ, Smyth GK. edgeR: a Bioconductor package for differential expression analysis of digital gene expression data. Bioinformatics. 2010; 26:139€140. [PubMed: 19910308]
60. Schmeier S, Alam T, Essack M, Bajic VB. TcoF-DB v2: update of the database of human and mouse transcription co-factors and transcription factor interactions. Nucleic Acids Res. 2017; 45:D145€D150. [PubMed: 27789689]
61. Parks DR, Roederer M, Moore WA. A new "Logicle" display method avoids deceptive effects of logarithmic scaling for low signals and compensated data. Cytometry A. 2006; 69:541€551. [PubMed: 16604519]
62. Lun AT, Chen Y, Smyth GK. It^s DE-licious: A Recipe for Differential Expression Analyses of RNA-seq Experiments Using Quasi-Likelihood Methods in edgeR. Methods Mol Biol. 2016; 1418:391€416. [PubMed: 27008025]
63. van der Maaten LJP. Accelerating t-SNE using tree-based algorithms. J Mach Learn Res. 2014; 15:3221€3245.

Europe PMC Funders Author Manuscripts

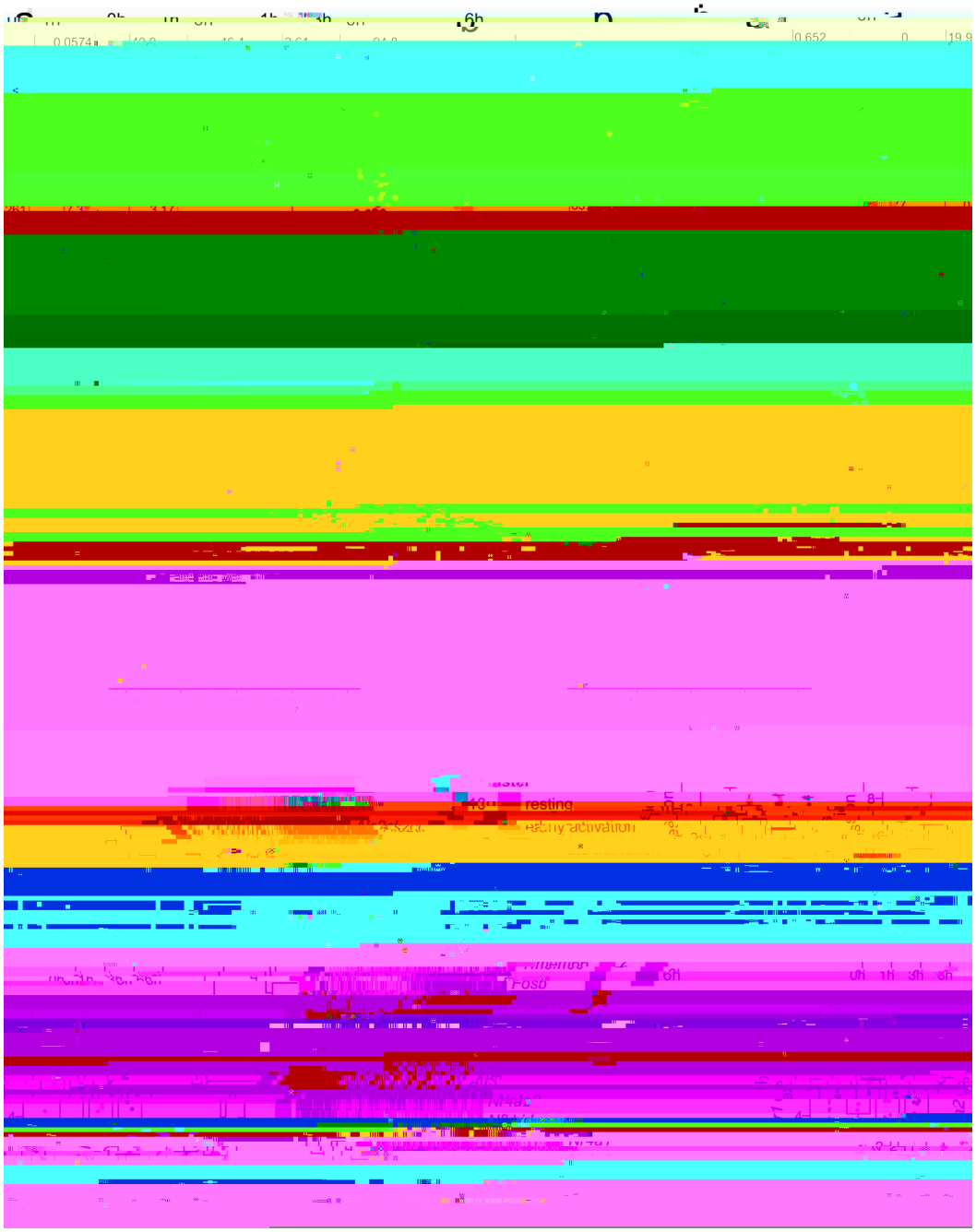

Fig. 1. A burst of transcriptional regulatory machinery characterizes early T cell activation.

a, OT-I CD8$^+$ T cells were stimulated with high potency ovalbumin peptide (N4) for 0, 1, 3, or 6 hours before sorting for scRNA-seq by FACS. Protein expression flow cytometry measurements are representative of at least 2 independent experiments. b, Principal components analysis of scRNA-seq of cells sorted in a. c, Diffusion pseudotime analysis of sequenced cells: cells are plotted by diffusion components (DCs) 1 and 2, with a black line delineating the pseudotime trajectory. Plot in c is colored by clusters in diffusion pseudotime. d, The top 20 genes transcriptionally upregulated in the early activation cluster

versus the resting and late activation clusters are depicted in a heatmap with genes clustered by Pearson correlation. Blue (TR) indicates transcriptional regulatory genes.

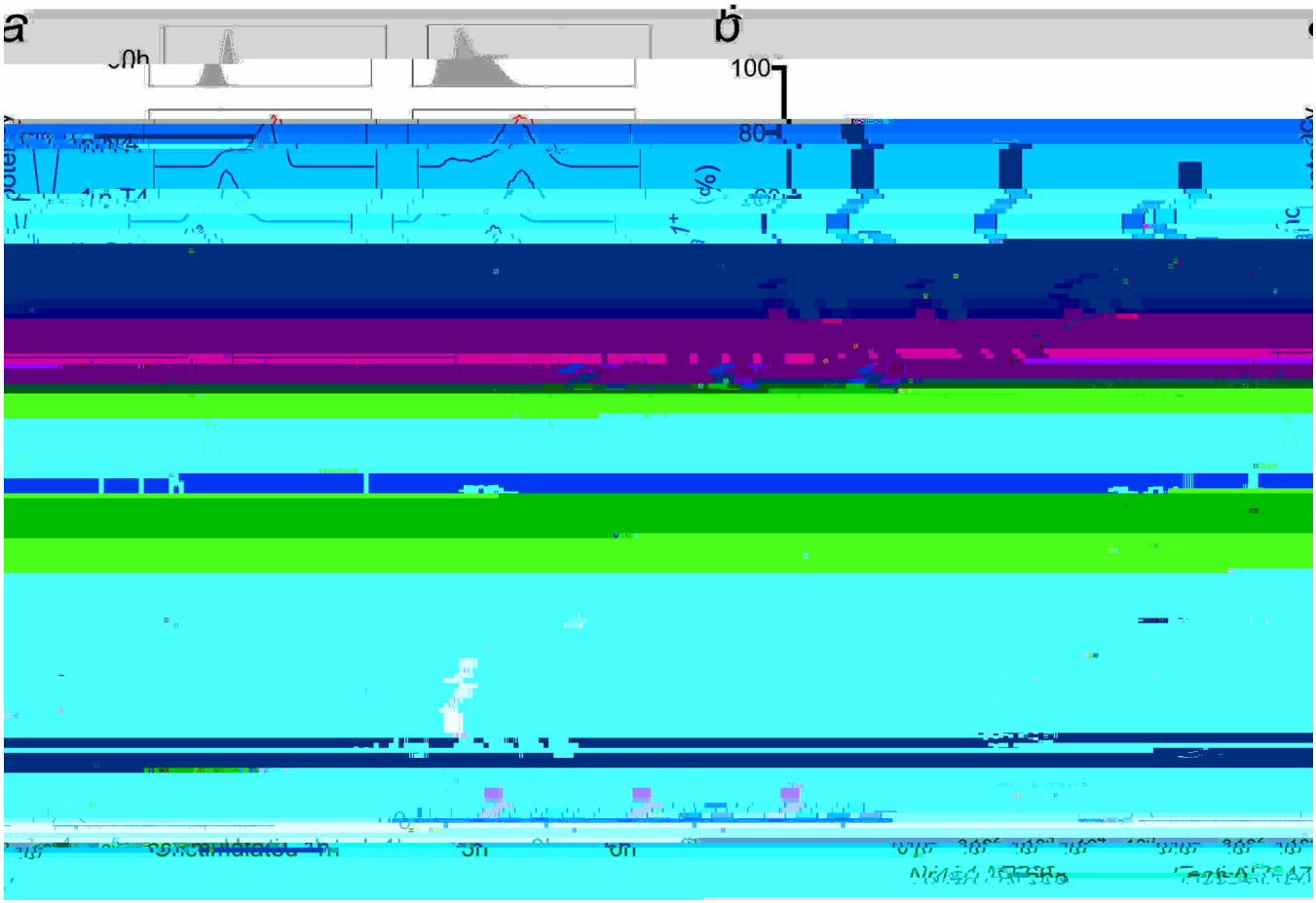

Fig. 2. Early response genes can be TCR-dependent or TCR-independent.
a, OT-I CD8$^+$ T cells were stimulated with high potency N4 peptide, reduced potency ligands (T4 or G4) or a non-binding control peptide (NP68) for the indicated times before examination of *Nr4a1* and *Fosb*

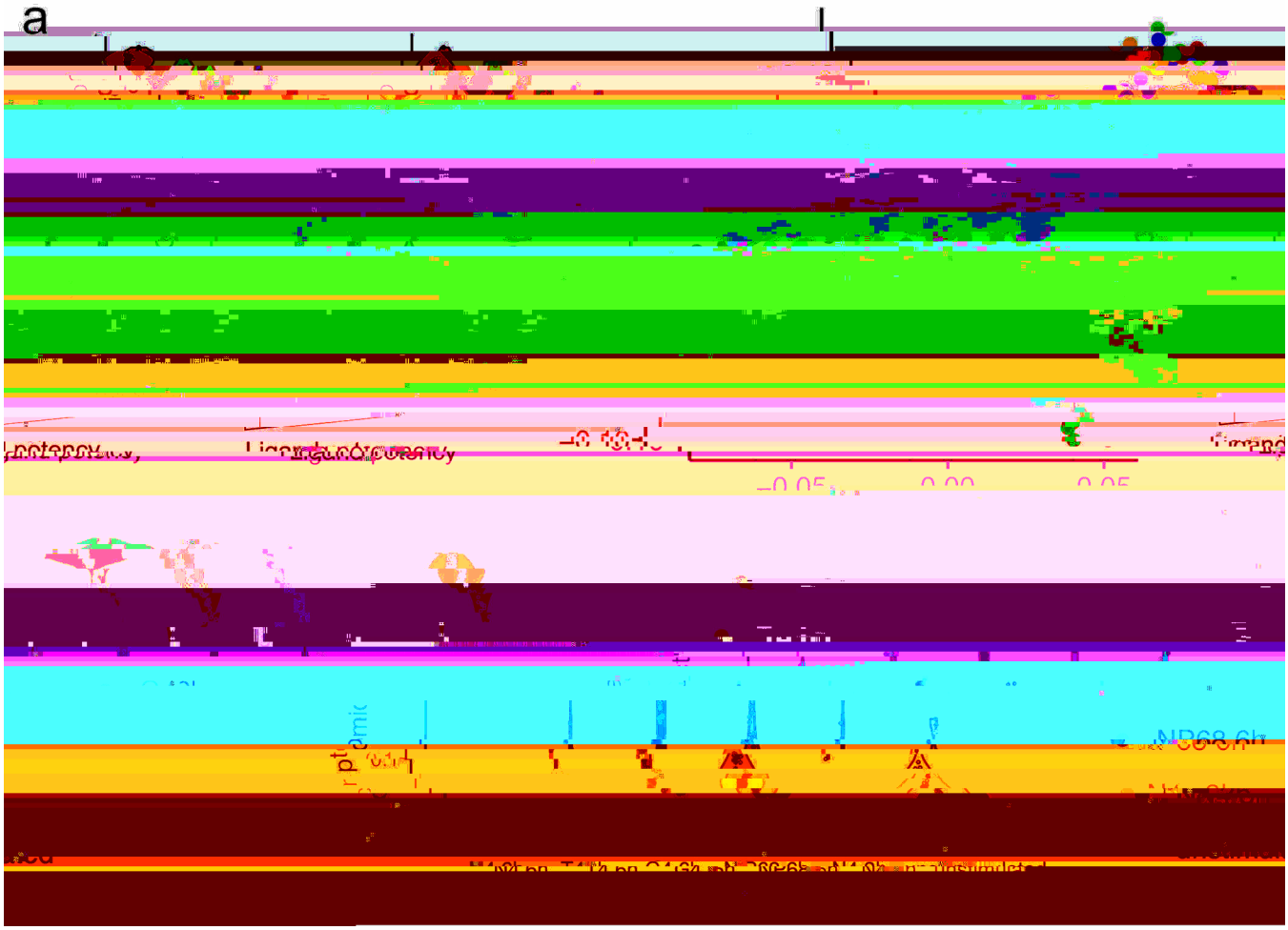

Fig. 3. Ligand potency determines activation rate.

OT-I CD8$^+$ T cells were stimulated for 6 hours with the various peptide ligands or for 3 hours with high affinity (N4) peptide for scRNA-seq. **a**, Violin plots depict the distribution of surface protein expression measurements in sequenced cells stimulated for 6 hours; n = 45 cells for N4, 44 for T4, 48 for G4, and 47 for NP68. A second independent experiment is depicted in Supplementary Fig. 3a. **b**, An activation trajectory was fit to the transcriptomic data by diffusion pseudotime analysis; n = 91 cells for N4 6h, 91 for T4 6h, 94 for G4 6h, 93 for NP68 6h, 64 for N4 3h, and 44 for unstimulated. Plot depicts combined data from two independent scRNA-seq experiments. **c**, Distribution of cells along the pseudotime transcriptomic activation trajectory fit in **b**, separated by stimulation condition.

Europe PMC Funders Author Manuscripts

Europe PMC Funders Author Manuscripts

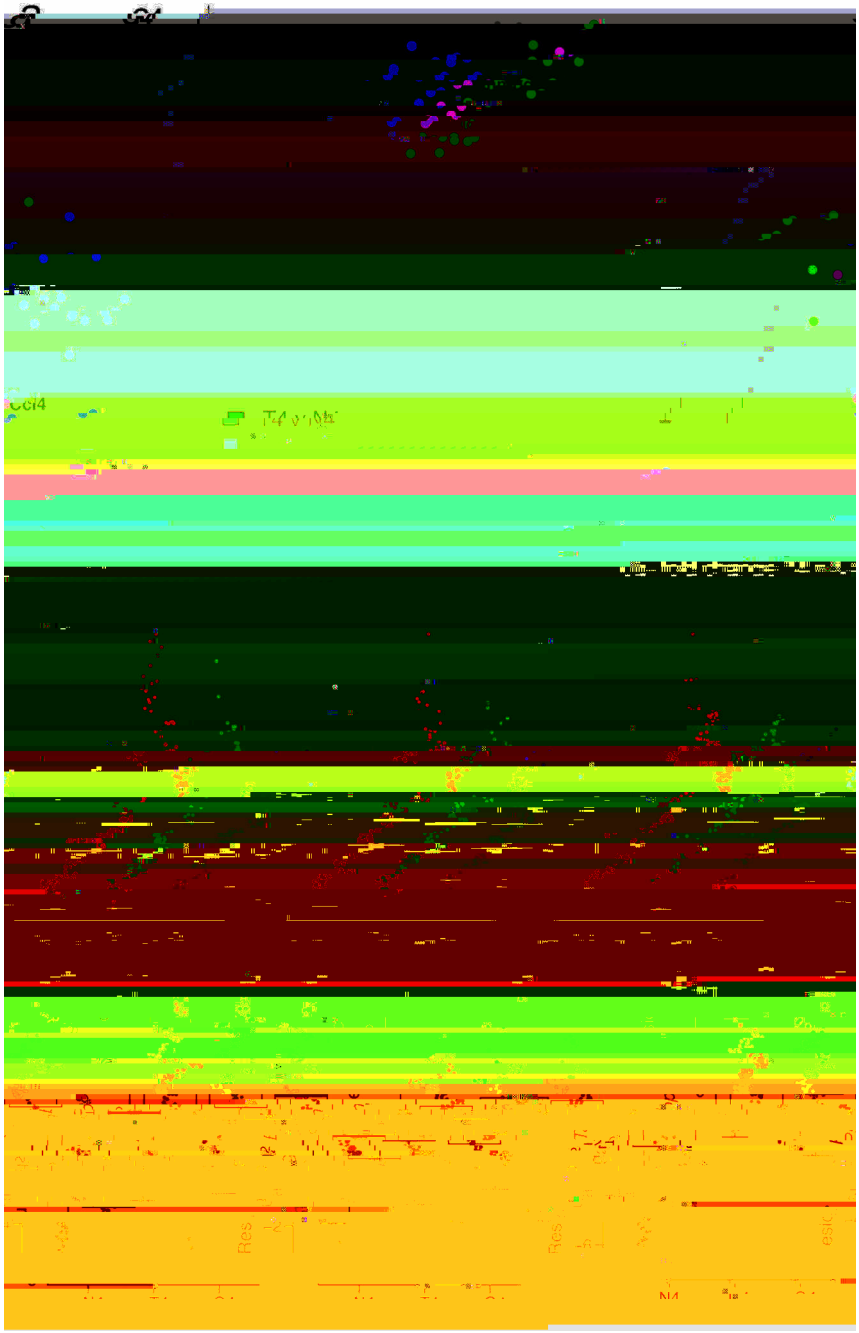

Fig. 4. Differential expression between cells activated by ligands of different potencies accounting for activation status.

a, Log_2-fold changes from a differential expression analysis between T4 (medium potency) and N4 (high potency), or G4 (low potency) and N4, peptide stimuli in Fig. 3, accounting for each cell's activation status as defined by log_{10} CD69 surface protein expression. Plot depicts all 8854 genes tested; differentially expressed genes (FDR < 0.05) for T4 versus N4 are shown in green; G4 versus N4, blue; intersection of T4 versus N4 and G4 versus N4, magenta and labelled. b, Residual expression of selected chemokine genes in scRNA-seq data after accounting for CD69 surface protein expression, plotted by stimulation condition.

Fig. 5. Cell number but not maximal division number is associated with ligand potency.
a

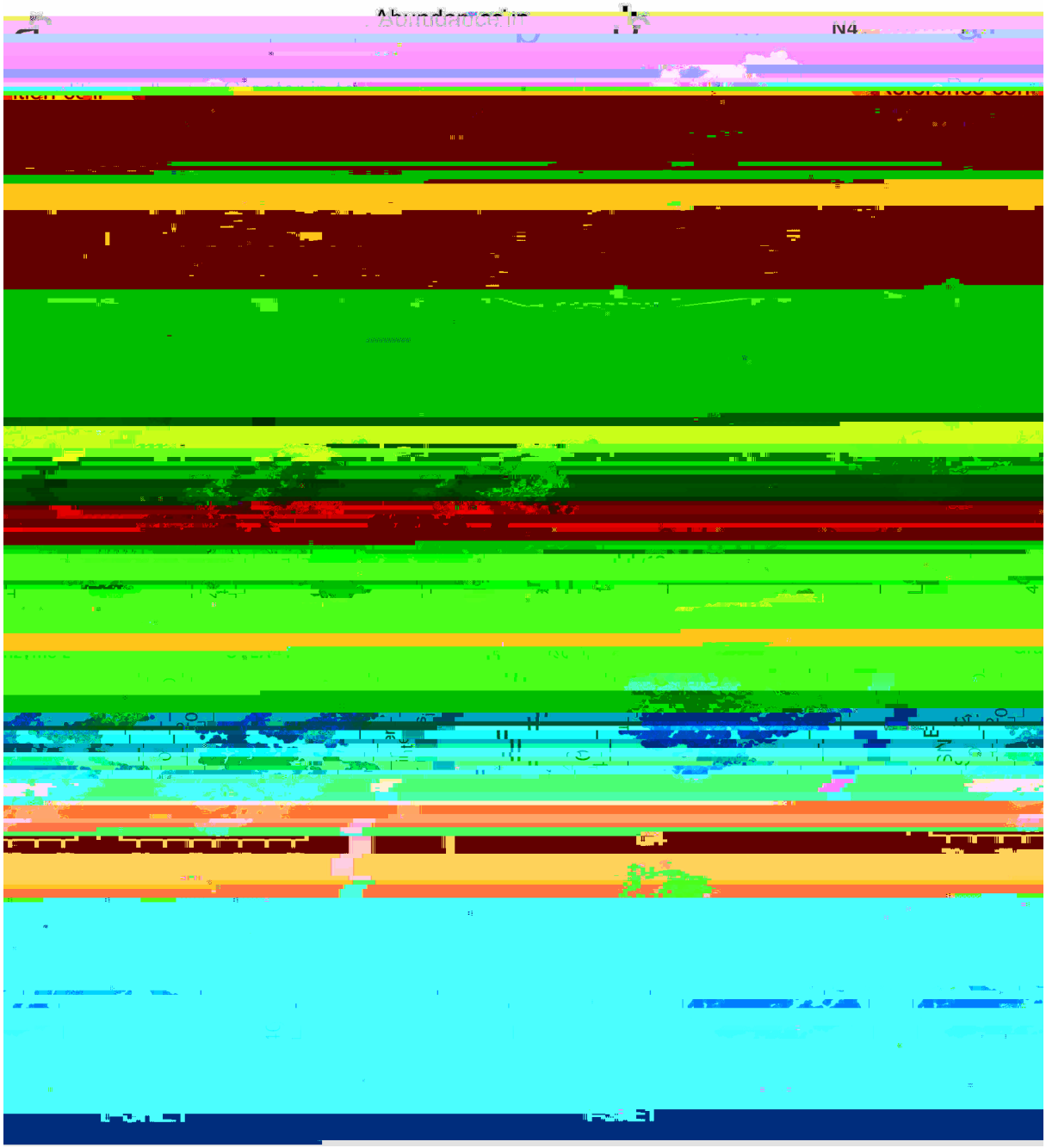

Fig. 6. Effector T cells exhibit the same spectrum of phenotypes, regardless of primary stimulation strength.

a, A schematic of differential abundance testing for mass cytometry data using cydar software demonstrates how cells are assigned to hyperspheres and how the abundance of cells within each hypersphere is compared between conditions.

abundant hyperspheres (FDR < 0.05, 5138 of 5160 tested), colored by the fold change in abundance between NP68 (null peptide) stimulation and the indicated ovalbumin peptide variant (statistical test described in Methods). The plot from b is colored by marker intensity for selected proteins.

Europe PMC Funders Author Manuscripts

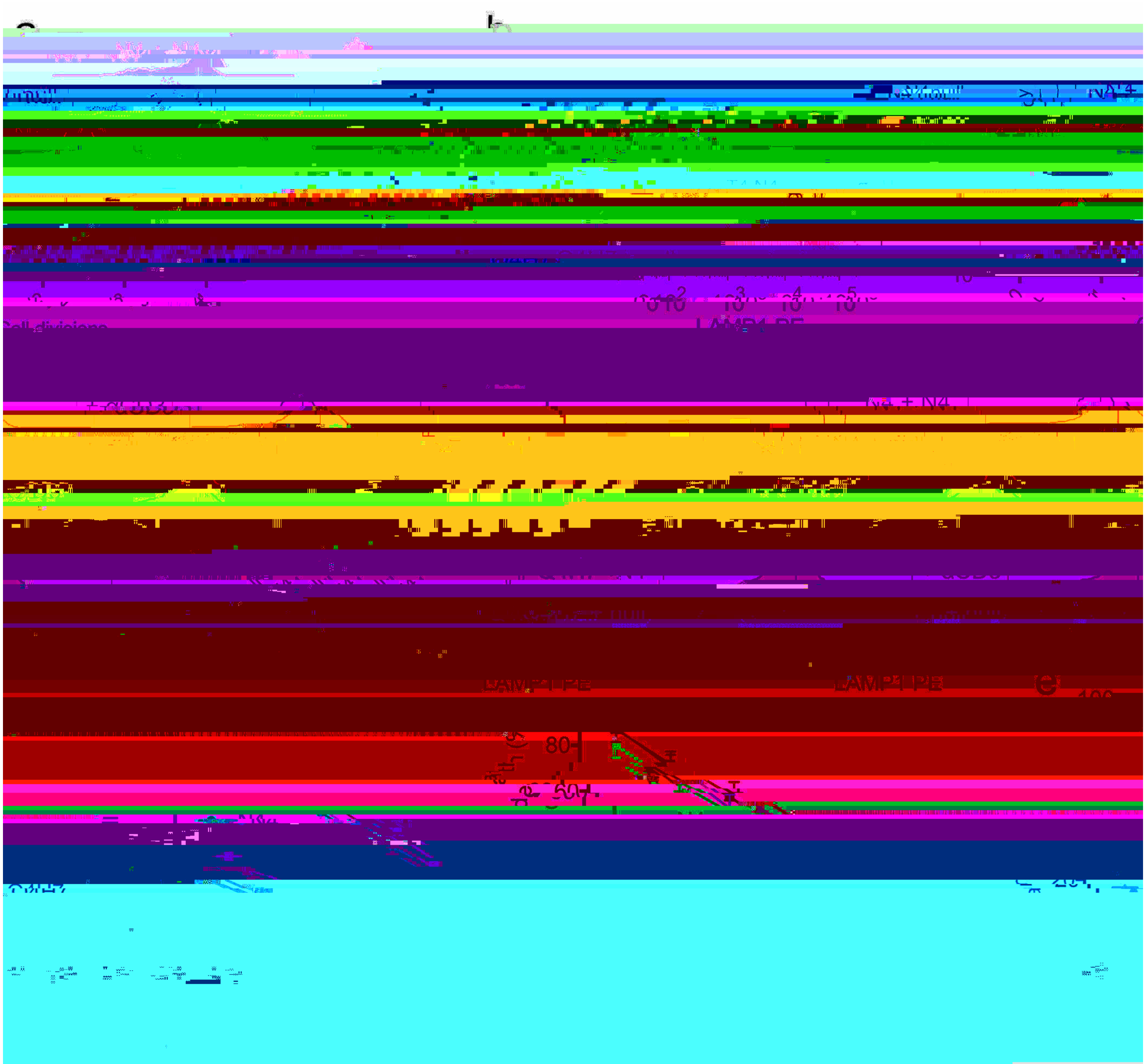

Fig. 7. All activated $CD8^+$ T cells can degranulate regardless of the affinity of their primary stimulus.

a, OTI $CD8^+$ T cells activated for 2 days as in Fig. 5 and 6 were challenged with high potency ovalbumin peptide (N4)-pulsed EL4 cells for 3 hours. Degranulation was quantified by adding anti-LAMP1 PE to the cell culture medium to measure lysosomal trafficking by flow cytometry. b, Cells in a were gated based on their proliferation dye intensity to identify those that had divided 0, 1, 2, 3, or 4 times before comparing LAMP1 median fluorescence intensity (MFI). c, As in b, $CD44^{hi}$ cells were gated before comparing LAMP1 MFI. Bar plots (b-c) depict mean of two technical replicates in one representative experiment. Results (a-b) are representative of 6 separate mice from 5 independent experiments and (c) 5 separate mice from 4 independent experiments. d, T cells stimulated as in a were cultured

for 7 days before a 3-hour challenge with ovalbumin peptide (N4)-pulsed EL4 cells (left) or plate-bound anti-CD3ε (right). Results are representative of 8 and 5 separate mice examined in 6 and 4 independent experiments, respectively. T cells activated as in vivo were cultured until day 8 and were tested for their ability to kill N4-pulsed EL4 cells by LDH release assay. Plot depicts combined data from 5 separate mice in 3 independent experiments; mean plotted with error bars representing SEM.